Please find the published version at:
https://www.sciencedirect.com/science/article/pii/S0196890420307548

Optimisation study of a supersonic separator considering nonequilibrium condensation behaviour

Chuang Wen[1], Hongbing Ding[2], Yan Yang[1, *]

[1]Faculty of Engineering, University of Nottingham, University Park, Nottingham NG7 2RD, UK

[2]Tianjin Key Laboratory of Process Measurement and Control, School of Electrical and Information Engineering, Tianjin University, Tianjin 300072, China

*Corresponding author: Yan Yang, Email: yan.yang1@nottingham.ac.uk; flyloveyang@gmail.com

Abstract: The supersonic separation offers an opportunity for natural gas processing. The problem is that the phase change of water vapour in the supersonic flow is not fully understood in the presence of shock waves in a supersonic separator. This study aims to evaluate the performance of the supersonic separation with the phase change process and shock waves. The condensing flow model is developed to accurately predict the energy conversion within the supersonic separator. The computational results show that the single-phase flow model over-estimates the vapour expansions by 12.43% higher Mach number than the condensing flow model. The liquid fraction of 8.2% is predicted by the condensing flow model during the phase change process in supersonic separators. The supersonic separator is optimised via combining the diverging part of the supersonic nozzle and constant cyclonic separation tube as a long diverging part of the newly designed nozzle. The optimised supersonic separator reduces the energy loss by eliminating the oblique and expansion waves in the newly designed nozzle, which

improves the energy efficiency for natural gas processing.

Keywords: supersonic separator, gas processing, supersonic flow, nonequilibrium condensation, condensing flow, phase change

1. Introduction

Clean utilisation of natural gas provides an opportunity to mitigate environmental pollutions [1]. A supersonic separator has been used for gas separation working on the phase change in supersonic flows and the strong centrifugal force owing to a swirling flow [2, 3]. The high-speed flow induces the low-pressure and low-temperature [4], which results in the nonequilibrium condensation of water vapour [5, 6]. The experiments have demonstrated that the hydrate does not form under low-pressure and low-temperature conditions [7]. Thus, a supersonic separator does not need any chemicals or inhibitors to prohibit hydration formation, which provides an environment-friendly way for natural gas processing.

The computational fluid dynamics (CFD) modelling has been employed for predicting the dehydration performance of the supersonic separator [8, 9], and most of them did not consider the phase change behaviour. Yang & Wen [10] assumed the size of the particles, which was released from the exit plane of the supersonic nozzle, to track the particle trajectories in a supersonic separator. Majidi & Farhadi [11] used a dry gas flow to study the influence of the drain structure on the position of the shock wave for the supersonic separation. Hu et al. [12] numerically investigated the flow structure in a supersonic separator with a reflow channel without considering nonequilibrium condensations.

A few studies were performed to simulate the water vapour phase change process within a supersonic separator, as shown in Table 1. In these numerical studies, Shooshtari & Shahsavand [13], Ma et al. [14, 15], Bian et al. [16, 17], Sun et al. [18, 19] developed a condensing flow model to investigate the phase change behaviour in a supersonic nozzle, but the shock wave was not involved in these simulations. Shooshtari & Shahsavand [20, 21] studied the phase change process in a supersonic separator using a mass transfer rate method for calculating the droplet growth with the one-dimensional model. Niknam et al. [22] investigated the phase change process of water vapour in a supersonic separator based on the evaporation-condensation model in ANSYS FLUENT. It can be seen that the phase change process is not fully understood in a supersonic separator.

Table 1 CFD studies on the supersonic separation with the phase change process

References	Models in the numerical study
Shooshtari & Shahsavand [13]	Condensing flow model, nozzle flow, no shock waves
Ma et al. [14, 15]	Condensing flow model, nozzle flow, no shock waves
Bian et al. [16, 17]	Condensing flow model, nozzle flow, no shock waves
Sun et al. [18, 19]	Condensing flow model, nozzle flow, no shock waves
Shooshtari & Shahsavand [20, 21]	Homogeneous nucleation and mass transfer rate calculations for liquid droplet growth
Niknam et al. [22]	Evaporation-condensation phase change model in ANSYS FLUENT

This study aims to assess the performance of the supersonic separation considering the phase change process and shock waves. A condensing flow model is developed for predicting the complicated fluid flow, heat and mass transfer of water vapour in the supersonic separator. The detailed analysis is performed to figure out the impact of nonequilibrium condensation behaviour on the supersonic separation using the single-phase flow and condensing flow models. The condensation parameters are described in detail within the supersonic separator including the nucleation rate, droplet radius and liquid fraction. The supersonic separator is optimised based on the condensing flow model to improve the separation performance and energy efficiency.

2. Mathematical modelling

2.1. Physical model

A typical supersonic separator is described in Fig. 1. The swirling flow generator is not involved in the present simulation to simplify the physical model by focusing on the condensation process in a supersonic separator. The Laval nozzle has a throat diameter of 14.70 mm, while the nozzle inlet and outlet diameters are 35.10 mm and 18.30 mm, respectively. The constant tube is installed to the exit plane of the Laval nozzle for the cyclonic separation. The outlet diameter of the diffuser is fixed at 40.00 mm. The dimension of the supersonic separator is shown in Table 2 [23].

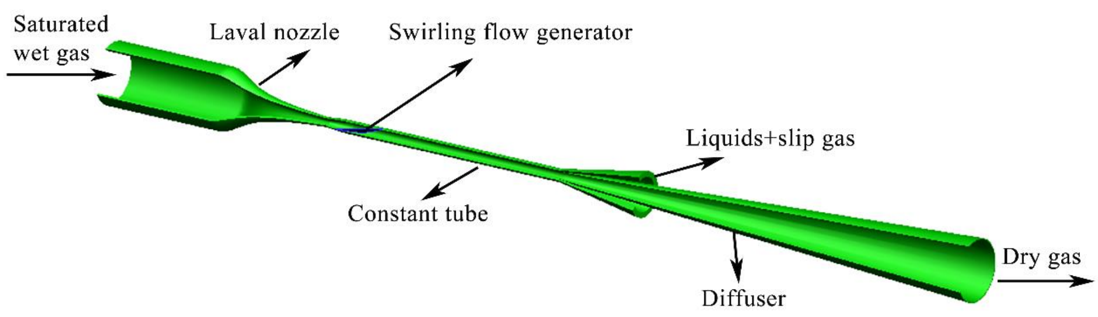

Fig. 1 Schematic of a supersonic separator

Table 2. The dimensions of a supersonic separator [23]

Dimensions	Value (mm)
Nozzle inlet diameter	35.10
Nozzle throat diameter	14.70
Nozzle outlet diameter	18.30
Length of nozzle converging part	33.39
Length of nozzle diverging part	73.50
Length of the constant tube	220.50
Outlet diameter of the diffuser	40.00
Length of the diffuser	206.85

2.2. Numerical model

The Eulerian approach is used for the flow prediction inside a supersonic separator involving the condensation process [24]. The liquid fraction (y) and droplet number (n) equations are employed to solve the phase change process in supersonic flows [25, 26]:

$$\frac{\partial(\rho y)}{\partial t}+\frac{\partial\left(\rho y u_j\right)}{\partial x_j}=\Gamma \tag{1}$$

$$\frac{\partial(\rho n)}{\partial t}+\frac{\partial\left(\rho n u_j\right)}{\partial x_j}=\rho J \tag{2}$$

where ρ is the mixture density, kg m^{-3}; u is the mixture velocity, m s^{-1}; y is the liquid fraction, dimensionless; n is the droplet number, m^{-3}; t is the time, s; J is the nucleation rate, m^{-3} s^{-1}; Γ is the mass generation rate due to the nonequilibrium condensation, kg m^{-3} s^{-1}, which is given [27, 28]:

$$\Gamma = \frac{4}{3}\pi r_c^{\,3}\rho_l J + 4\pi r^2 \rho_l n \frac{dr}{dt} \tag{3}$$

where r_c is the critical droplet radius, m; r is the droplet radius, m; ρ_l is the liquid density, kg m^{-3}; dr/dt is the growth rate of the condensed droplet, m s^{-1}.

The classical nucleation theory is used to calculate the nucleation rate [29]:

$$J = \frac{q_c}{1+\phi}\frac{\rho_v^{\,2}}{\rho_l}\sqrt{\frac{2\sigma}{\pi m_v^{\,3}}}\exp\left(-\frac{4\pi\sigma}{3k_B T_v}r_c^{\,2}\right) \tag{4}$$

where ρ_v is the vapour density, kg m^{-3}; m_v is the mass of a vapour molecule, kg; T_v is the vapour temperature, K; σ is the surface tension, N m^{-1}; k_B is the Boltzmann's constant, J K^{-1}. q_c and ϕ are the model parameters, dimensionless.

The Young's model is used to calculate the droplet growth rate [30, 31]:

$$\frac{dr}{dt} = \frac{\lambda_v \Delta T}{\rho_l h r}\frac{\left(1 - r_c/r\right)}{\left(\frac{1}{1+2\beta \mathrm{Kn}} + 3.78(1-\nu)\frac{\mathrm{Kn}}{\mathrm{Pr}}\right)} \tag{5}$$

$$\Delta T = T_s - T_v \tag{6}$$

where λ_v is the vapour conductivity, W m^{-1} K^{-1}; T_s is the saturation temperature, K; ΔT is the degree of supercooling, K; h is the enthalpy, J kg^{-1}; β and ν are the model parameters, dimensionless; Pr is the Prandtl number, dimensionless; Kn is the Knudsen number, dimensionless.

2.3. Model implementation

For the single-phase flow modelling, the continuity, mass and energy conservation equations are directly solved by ANSYS FLUENT 18 [32], and these well-known equations are not shown for simplicity. For the condensing flow modelling, the liquid fraction (y) and droplet number (n) equations, as well as the Eqs. (3) – (6) are solved using C programming [33] to describe the nonequilibrium condensation process in a supersonic separator. For the calculation of the phase change process, the nucleation process starts to generate massive critical radius droplets when the vapour reaches the nonequilibrium state. When the droplet radius is greater than the critical one, the droplet growth process is initiated to form bigger droplets. The mass transfer between the vapour and liquid phases comes from the nucleation and droplet growth processes. The shear stress transport (SST) k-ω turbulence model [34, 35] is adopted considering the supersonic flow [36] and nonequilibrium condensations [37]. The thermophysical properties like the density [38], viscosity [39], specific heat capacity [40] and thermal conductivity [41] are used from the Fluent library, while the saturation pressure, saturation temperature, surface tension, and density of water liquid are developed by the UDF during the numerical simulation.

The structured grid is employed for the designed supersonic separator, as shown in Fig. 2. The boundary conditions for the supersonic separator are described in Table 3. The mesh independence is investigated based on 19500, 36000 and 66250 structured cells for coarse, medium and fine meshes, respectively. Figure 3 describes the Mach numbers and liquid fraction in the flow and longitudinal directions. The Mach number is defined as the ratio of the flow velocity to the local speed of sound. Three different grid resolutions represent almost the same flow behaviour both in the flow and longitudinal directions upstream the shock wave. This indicates that these grids capture the occurrence of the nonequilibrium condensation in the supersonic separator. However, the difference is observed when the shock wave appears. The Mach number and liquid fraction from the coarse mesh diverge from those of medium and fine meshes, which shows that the coarse mesh is not enough for predicting a shock wave. Therefore, the medium mesh is used for evaluating the dehydration performance of a supersonic separator considering the numerical cost and time.

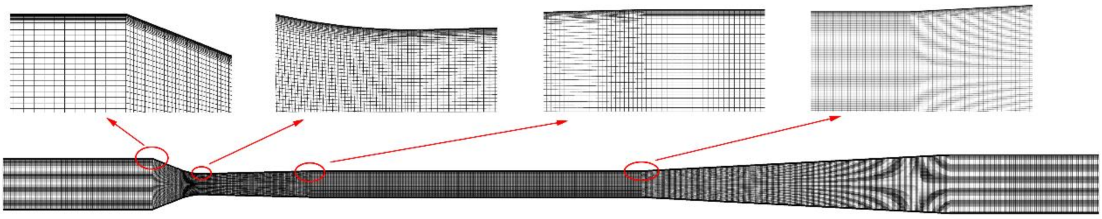

Fig. 2 Numerical grid for a supersonic separator

Table 3 Boundary conditions for the supersonic separator

Boundary conditions	Separator inlet	Separator outlet	Walls and fluids
Total pressure	40 bar	25 bar	Working fluids: water vapour
Total temperature	520 K	520 K	No-slip, adiabatic walls

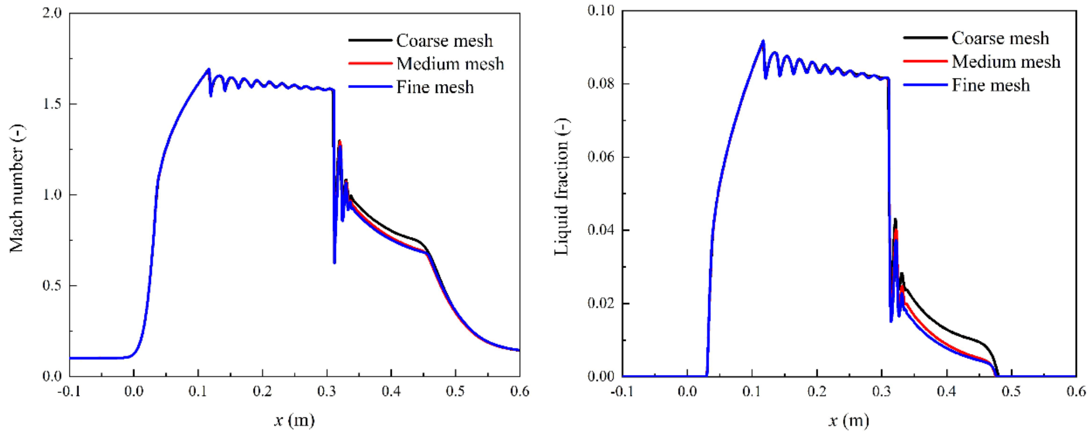

(a) Mach number and liquid fraction along the flow direction

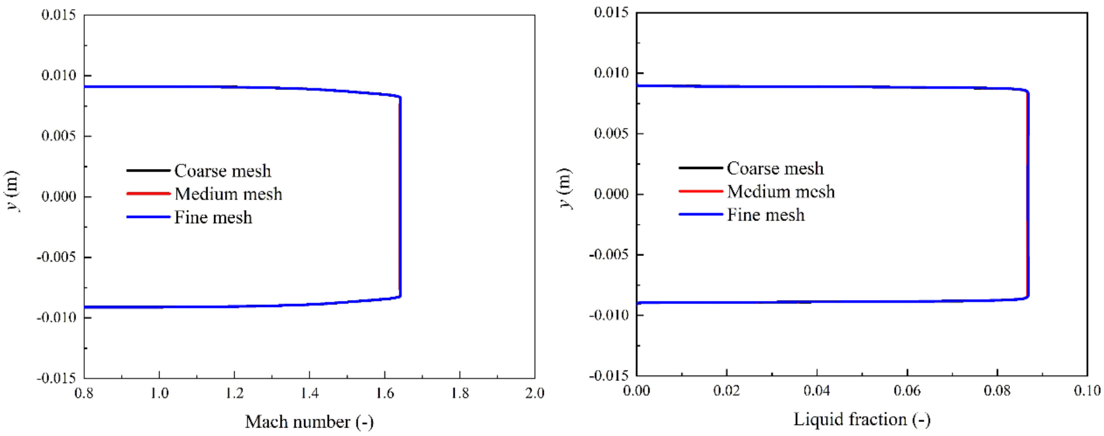

(b) Mach number and liquid fraction at the exit plane of the supersonic nozzle

Fig. 3 Impact of the grid resolution on the condensation flow in a supersonic separator

3. Results and discussion

3.1. Model validation

The developed condensing flow model is validated against experimental data [42]. The static pressure and droplet radius inside the Laval nozzle are shown in Fig. 4. The results indicate that the developed CFD model predicts accurately the flow and condensation behaviours in supersonic flows. The CFD model captures the onset of the condensation shock due to the heat and mass transfer during the phase change process. To compare the numerical and experimental results, the root-mean-square (R^2) is employed to determine the error between them [43-45], which is defined in Eq. (7). The root-mean-square (R^2) for the static pressure and droplet radius between the experimental and numerical results can reach 0.99. The correlations (root-mean-square-R^2) between the experimental and numerical static pressure and droplet radius are shown in Fig. 4 (c) and (d), respectively. It can be seen that good compliance between the experimental and numerical static pressure is obtained. For the droplet radius, the upstream two numerical data deviate significantly from the experimental data, while others agree well with each other. Generally, the numerical results can reflect the experimental data very well. Thus, it can be concluded that the developed condensing flow model can be used to evaluate the flow features in the supersonic separator.

$$R^2 = 1 - \frac{\sum_{i=1}^{n} \left(a_i - p_i\right)^2}{\sum_{i=1}^{n} \left(p_i\right)^2} \tag{7}$$

where a_i is the experimental value, p_i is the numerical value, and n is the output data number.

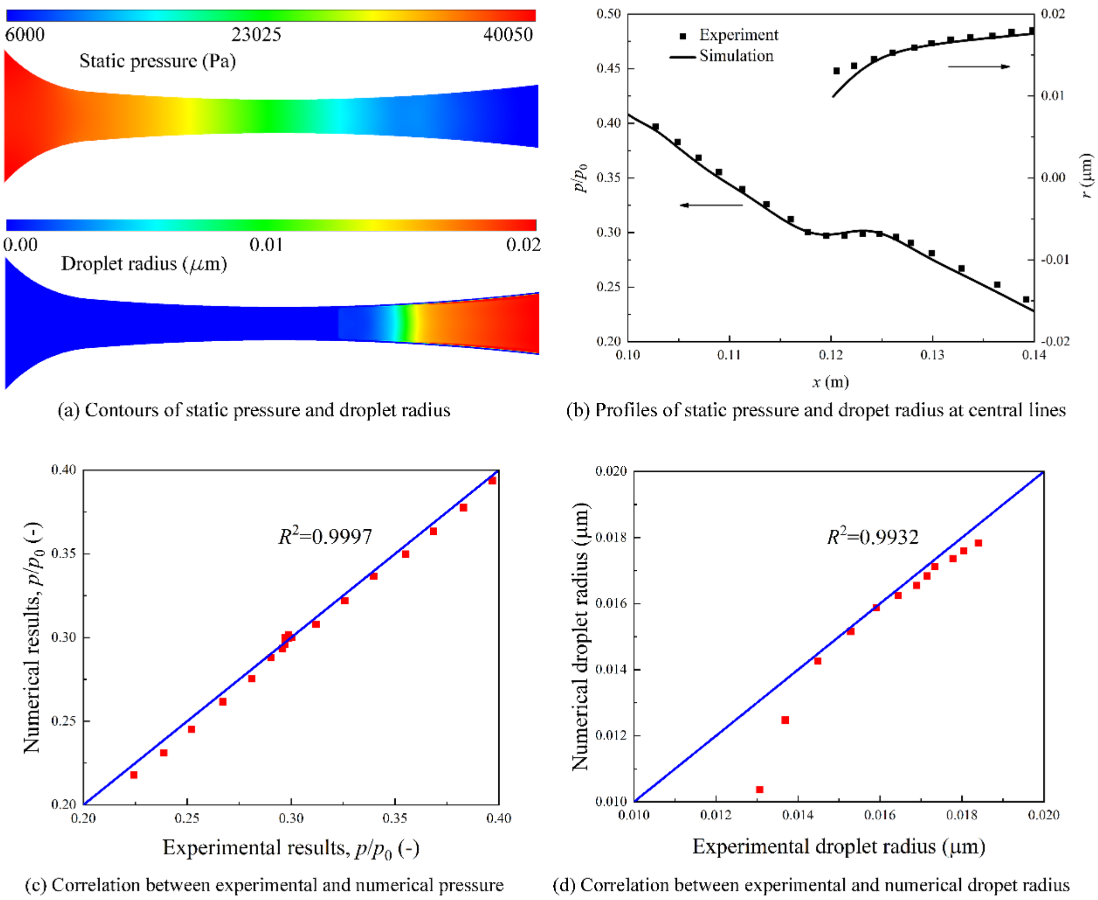

(a) Contours of static pressure and droplet radius

(b) Profiles of static pressure and dropet radius at central lines

(c) Correlation between experimental and numerical pressure

(d) Correlation between experimental and numerical dropet radius

Fig. 4 CFD validation of the nonequilibrium condensation in supersonic flows: total pressure and temperature at nozzle inlet: 40.05 kPa and 374.3 K

3.2. Flow features in supersonic separators by single-phase flow and condensing flow models

The Mach number, static pressure and static temperature are described in Figs. 5-7 based on the single-phase flow and condensing flow models. The two models predict almost the same flow behaviour upstream the nozzle throat, where water vapour is accelerated with the increase of the Mach number. The choked flow is obtained at the nozzle throat and then the supersonic flow is achieved in the nozzle diverging part. The Mach number achieves the peak value at the nozzle exit plane. The supersonic flow is obtained in the constant tube both for the single-phase flow and condensing flow models, where the Mach number is greater than 1.5. The shock wave occurs in the diffuser when the back pressure is fixed at 62.5% of inlet pressure. The static pressure is recovered as the subsonic flow is achieved downstream the shock wave. This improves the energy efficiency for the supersonic separation.

The different flow behaviours of the Mach number, static pressure and static temperature, are observed downstream the nozzle throat between the single-phase flow and condensing flow models. The Mach number predicted by the single-phase flow model is greater than that of the condensing flow model. The maximum Mach number at the nozzle exit plane is 1.90 for the single-phase flow assumption compared to 1.69 for the condensing flow model. This indicates that the single-phase flow model over-estimates the expansion capacity of the Laval nozzle of 12.43% higher than the condensing flow model.

For the single-phase flow model, the static temperature declines continuously in the diverging part of the Laval nozzle without considering the supersaturation state of water vapour. On the contrary, the condensing flow model causes a rise of the static temperature downstream the nozzle throat. This indicates that the latent heat is released to heat the vapour phase during the nonequilibrium condensation process in a supersonic separator.

Furthermore, the single-phase flow and condensing flow models compute different shock waves in the supersonic separator, such as the position and intensity of the shock waves. On one hand, the single-phase flow model predicts an earlier shock position compared to the condensing flow model, which shifts the shock position upward the

Laval nozzle. Under this operating condition, the single-phase flow model under-predicts the dehydration performance of the supersonic separation. For instance, the shock wave occurs in the diffusers for this design according to the condensing flow model, which is a normal condition for water vapour separation in supersonic separators. However, the single-phase flow model moves the shock position upward and the shock wave occurs in the constant tube, where the supersonic separator does not work as the abrupt rises of the static pressure and temperature because it can cause the re-evaporation of the condensed droplets. On the other hand, the condensing flow model weakens the intensity of the shock wave compared to the single-phase flow assumption, which can be observed from the drops of the Mach number and rises of the static pressure and temperature. This suggests that the condensing flow model improves the prediction of the pressure recovery in a supersonic separator.

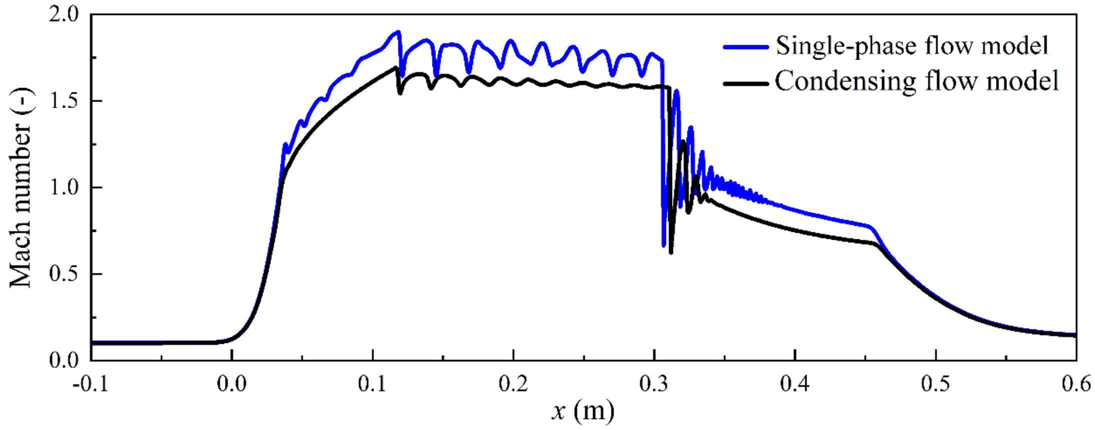

(a) Profiles of Mach number at the central line

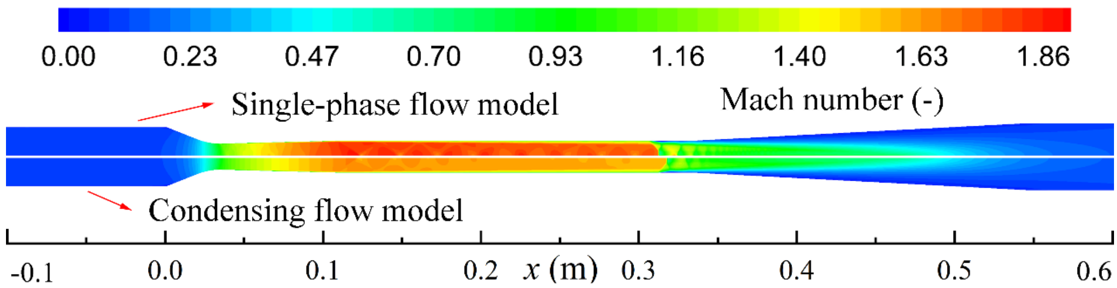

(b) Contours of Mach number in supersonic separators

Fig. 5 Mach number in supersonic separators with and without the condensation process

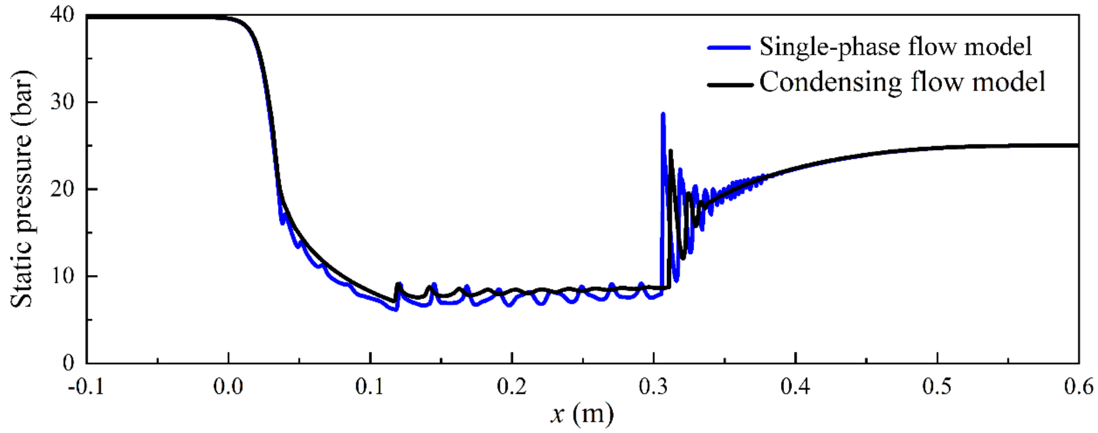

(a) Profiles of static pressure at the central line

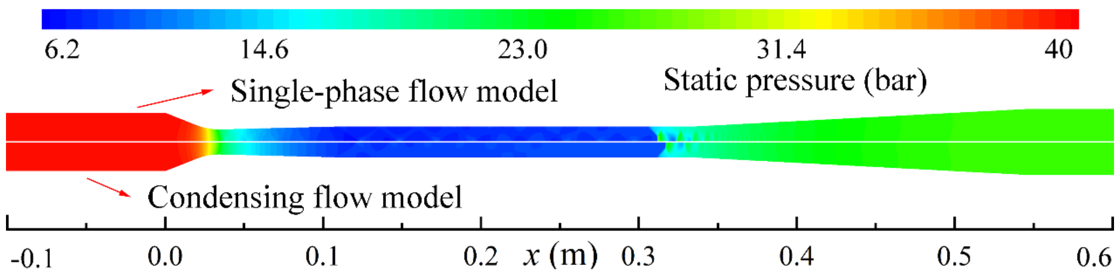

(b) Contours of static pressure in supersonic separators

Fig. 6 Static pressure in supersonic separators with and without the condensation process

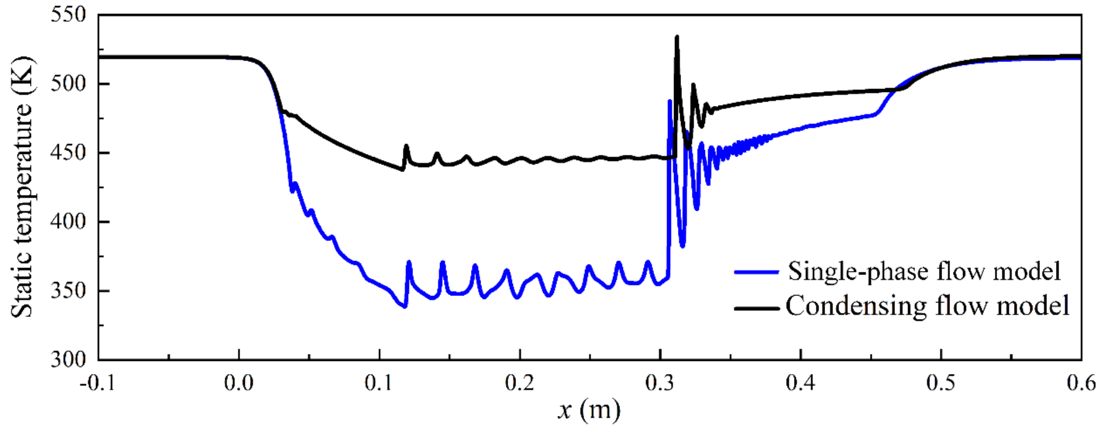

(a) Profiles of static temperature at the central line

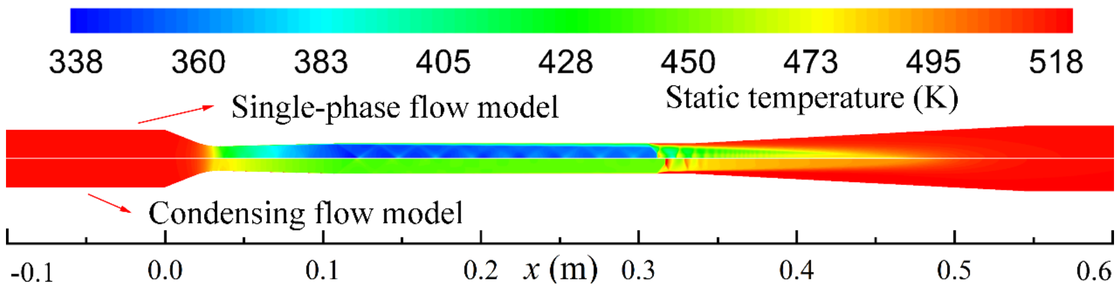

(b) Contours of static temperature in supersonic separators

Fig. 7 Static temperature in supersonic separators with and without the condensation process

3.3. Condensation phenomenon in supersonic separators

The condensation parameters during water vapour removal in the designed supersonic separators are shown in Figs. 8-11, including the degree of supercooling, nucleation rate, droplet radius and liquid fraction, respectively. Fig. 8 implies that the degree of supercooling increases with the vapour expansion in the Laval nozzle, which can reach a peak value of approximately 23 K in the designed supersonic separator. The extremely nonequilibrium state of water vapour induces the homogenous nucleation in supersonic flows. The degree of supercooling fluctuating around zero in the constant tube indicates that the latent heat is released to the vapour phase, which makes the vapour return to the quasi-equilibrium state. The shock wave induces an overly unsaturated state of water vapour with the degree of supercooling of -46 K, which will cause the re-evaporation of the condensed droplets in the diffuser.

The maximum nucleation rate of 8.59×10^{22} m^{-3} s^{-1} occurs in the nozzle diverging part of the supersonic separator, as shown in Fig. 9. The nonequilibrium nucleation induces the appearance of a great number of nuclei, which allows the vapour molecules to condense on the nucleus surface. It, therefore, induces the growth of the size of the condensed droplets, which can be observed from the distribution of the droplet radius at x = 0.028 mm -0.044 mm, as shown in Fig. 10. The maximum value of the droplet radius is approximately 0.08 μm in the designed supersonic separator. The liquid fraction increases and achieves the maximum value of about 9.2% of the total mass, which decreases downstream the exit plane of the Laval nozzle and stays at around 8.2% in the constant tube, as shown in Fig. 11. As expected, the liquid fraction declines suddenly as a result of the shock wave, which increases the static pressure and temperature. This indicates that the condensed liquids re-evaporate completely at the separator outlet if they enter into the diffuser, which should be removed by the strong centrifugal force induced by the swirling flow generator (ignored in this study).

In addition, the fluctuation of the profiles both from the flow structure and the condensation parameters, such as Mach number, static pressure and liquid fraction, was not observed in the Moses and Stein experiments [42]. It shows that the oblique and expansion waves occur in the supersonic separator, which are not expected for the removal of water vapour. These shocks and waves generate the shock trains in the constant tube, which increases the energy loss and leads to the decrease of the separation efficiency. The reasons are that the constant tube is placed to the nozzle exit without a smooth transition. An intersection angle forms between the straight profiles of diverging part of the Laval nozzle and the constant tube. This indicates that the connection of the Laval nozzle and constant tube needs to be designed specifically to avoid the shock trains for the removal of water vapour in supersonic separators.

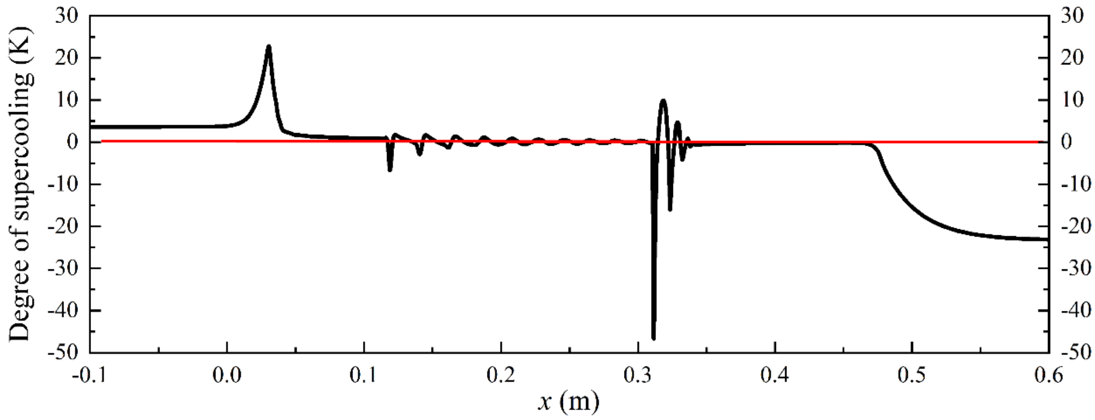

(a) Profile of degree of supercooling at the central line of the supersonic separator

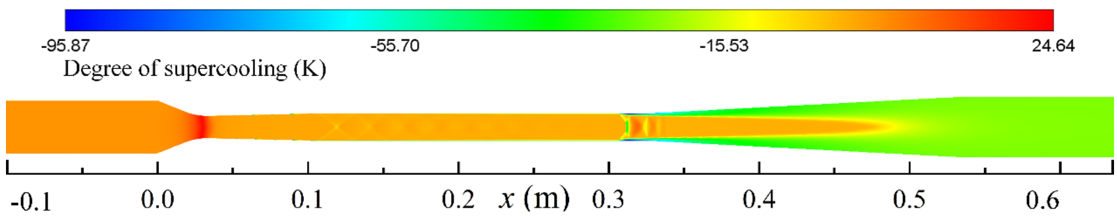

(b) Contour of degree of supercooling in the supersonic separator

Fig. 8 Degree of supercooling in the supersonic separator

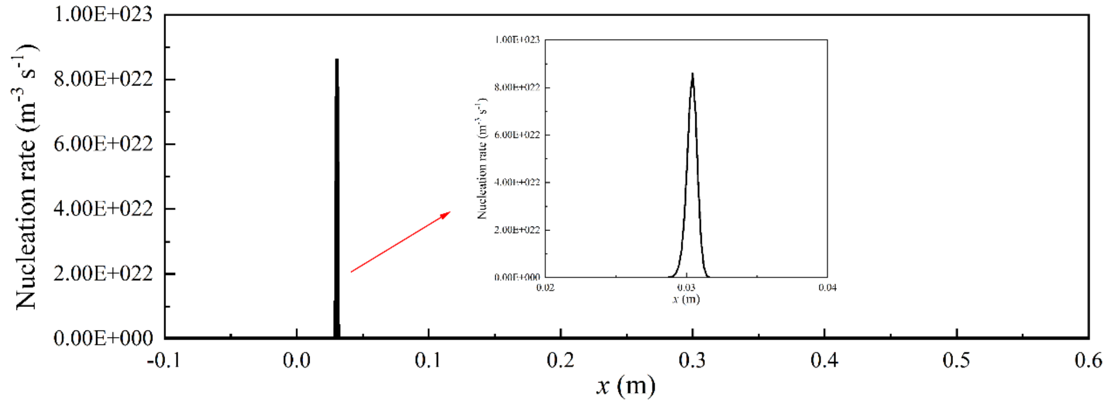

(a) Profile of nucleation rate at the central line of the supersonic separator

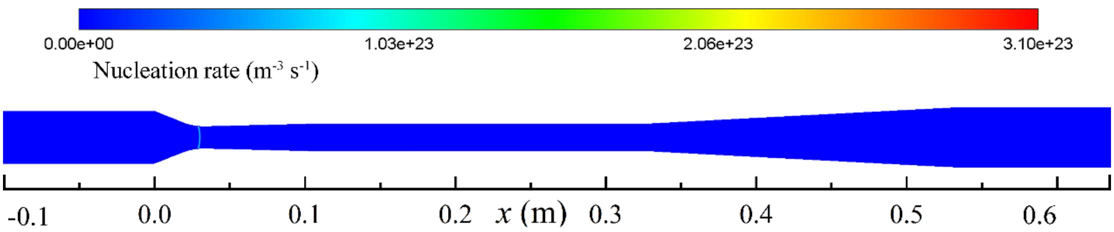

(b) Contour of nucleation rate in the supersonic separator

Fig. 9 Nucleation rate in the supersonic separator

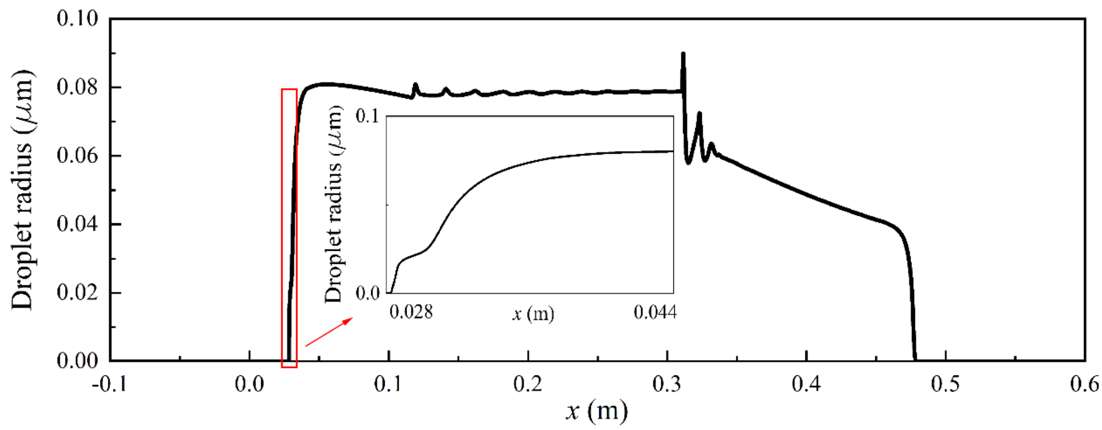

(a) Profile of droplet radius at the central line of the supersonic separator

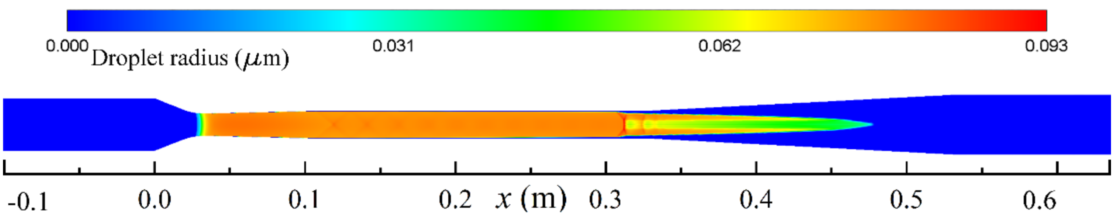

(b) Contour of droplet radius in the supersonic separator

Fig. 10 Droplet radius in the supersonic separator

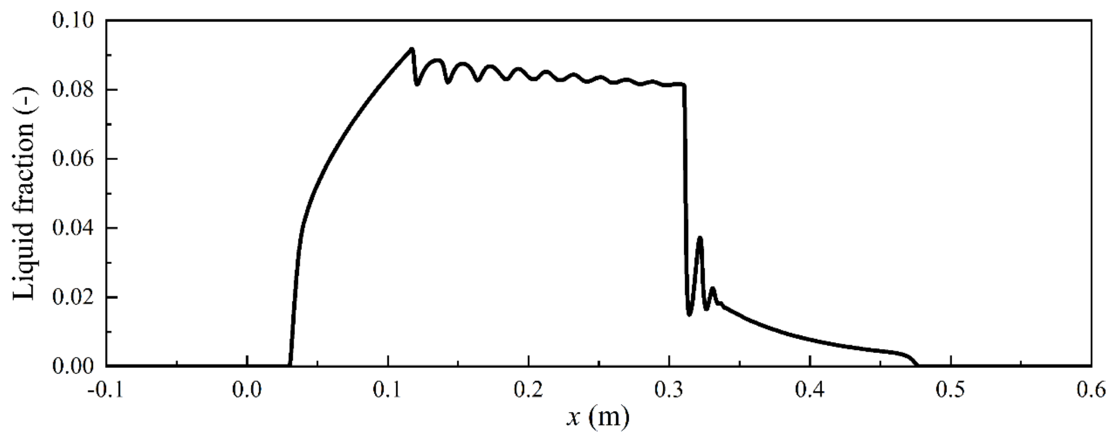

(a) Profile of liquid fraction at the central line of the supersonic separator

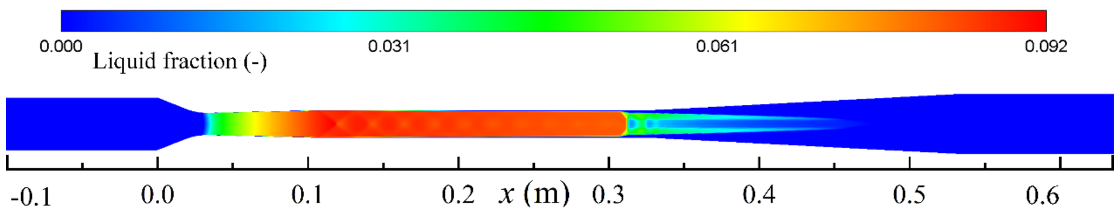

(b) Contour of liquid fraction in the supersonic separator

Fig. 11 Liquid fraction in the supersonic separator

3.4. Optimisation of the supersonic separator

To mitigate the energy loss due to the oblique and expansion waves in the constant tube as mentioned above, the supersonic separator is optimised based on the idea of combining the diverging part of the Laval nozzle and the constant tube as a long diverging section of the new nozzle, which is expected to eliminate the flow fluctuation. The schematic diagrams of original and optimised geometries are illustrated in Fig. 12.

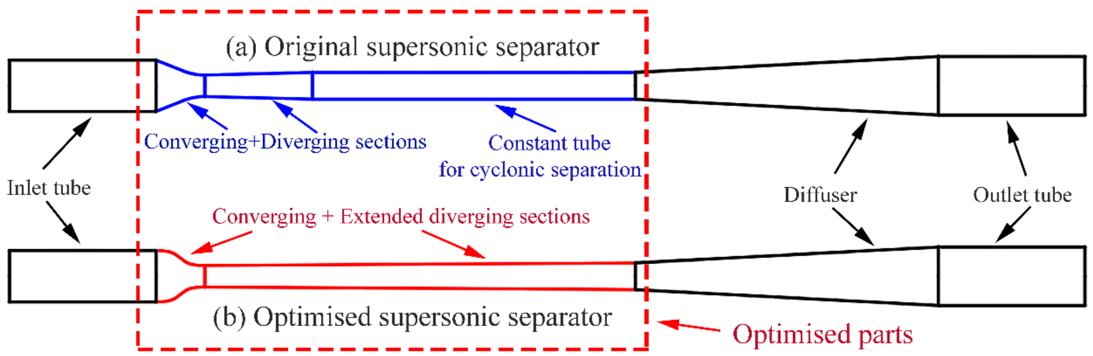

Fig. 12 Schematic diagram of the original and optimised supersonic separators

The detailed comparison of the flow and condensation parameters are described in Figs. 13-17, including the Mach number, degree of supersaturation, nucleation rate, droplet radius and liquid fraction. The Mach number in the original and optimised supersonic separators presents that the vapour expands uniformly in the long diverging part of the new nozzle compared to the original geometry which gives a faster expansion and generates oblique and expansion waves. The fluctuation of the profiles is not observed within the optimised supersonic separator, meaning that the oblique and expansion waves disappear in the newly designed device.

The degree of supersaturation, which is defined as the ratio of the vapour pressure to the saturation pressure, moves forwards the nozzle entrance in the optimised supersonic separator compared to the one in the original geometry. This means that the extremely nonequilibrium state occurs earlier in the optimised supersonic separator. It, therefore, causes an earlier onset of the nucleation process as described in Fig. 15. Accordingly, the optimised maximum value of the nucleation rate declines to 6.13×10^{22} m^{-3} s^{-1} compared to 8.59×10^{22} m^{-3} s^{-1} in the original geometry. When looking into the details of the growth process of the condensed droplets, it can be seen that the optimised geometry leads to an earlier onset of the formation of the liquid droplet. This demonstrates that an earlier nucleation process induces an earlier formation of the droplets. The optimized supersonic separator presents larger sizes of the condensed droplet compared to the original one. Fig 17 reveals that the optimised geometry induces an earlier onset of the liquid fraction compared to the original supersonic separator. The liquid fraction then increases uniformly inside the long diverging section of the newly designed nozzle in the optimised supersonic separator, which generates a maximum liquid fraction of approximately 0.084 of the total mass.

Furthermore, the profiles of the flow and condensation parameters depict that the shock position inside the optimised separator moves downstream compared to the one in the original geometry. The profiles of the Mach number and degree of supersaturation illustrate that the optimised supersonic separator weakens the intensity of the shock waves. The optimised idea of combining the nozzle diverging part and the constant tube as a long diverging part of the newly designed nozzle reduces the energy loss due to the oblique and expansion waves and improve the energy efficiency of the supersonic separation.

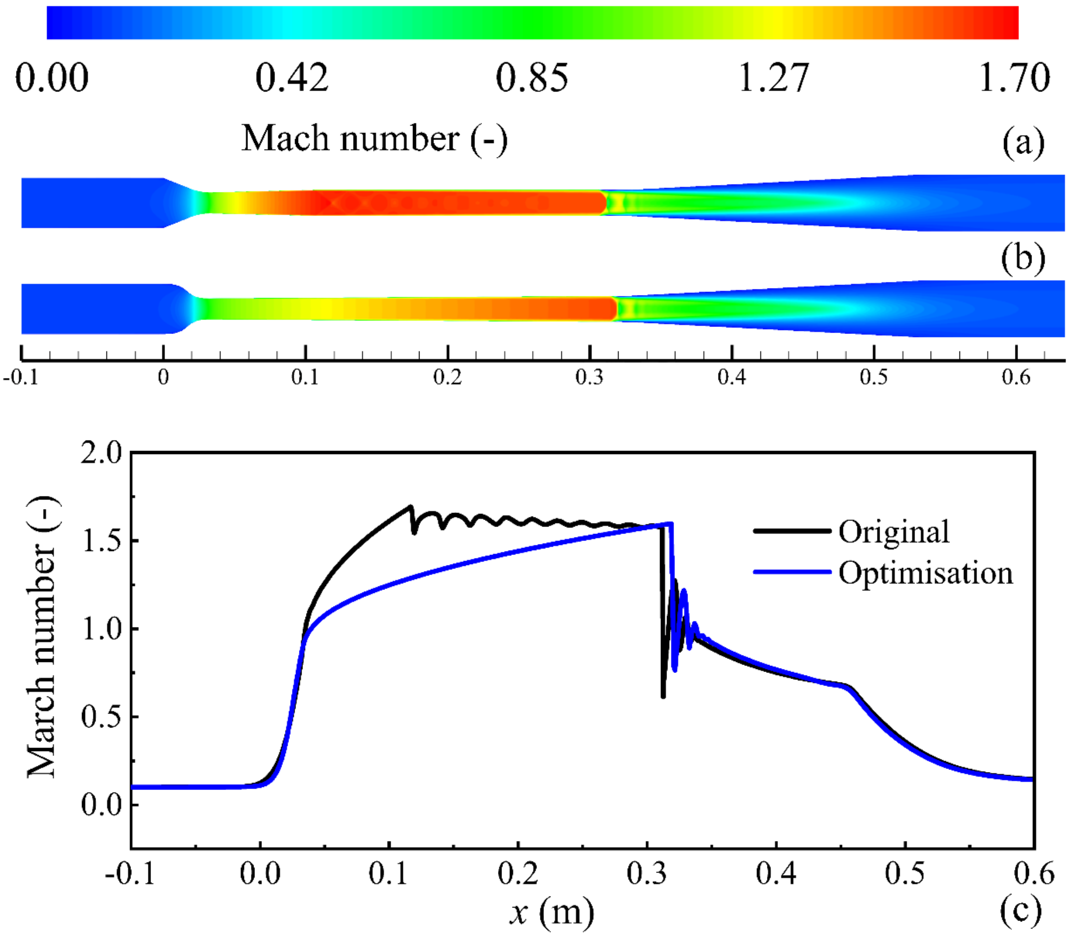

Fig. 13 Mach number in original and optimised supersonic separators: contours of the

original geometry (a), contours of the optimised geometry (b) and profiles of the original and optimised geometries (c)

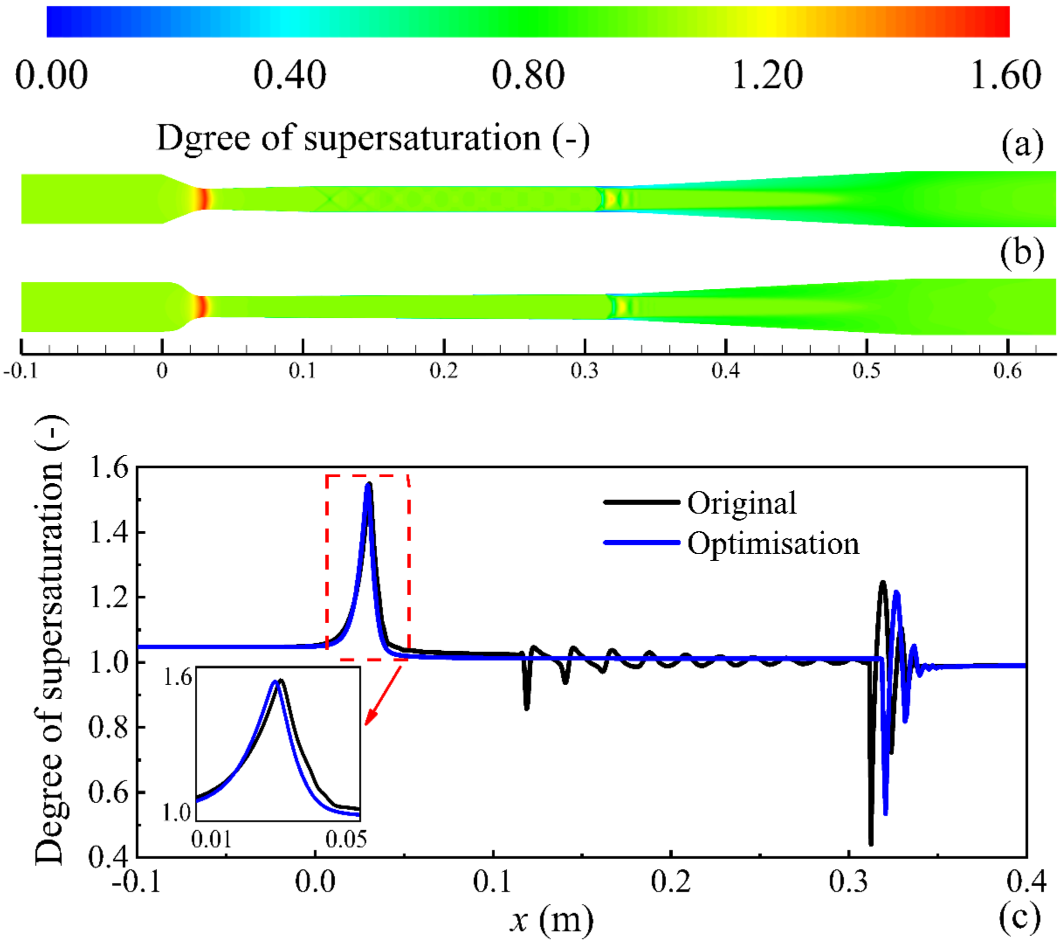

Fig. 14 Degree of supersaturation in original and optimised supersonic separators: contours of the original geometry (a), contours of the optimised geometry (b) and profiles of the original and optimised geometries (c)

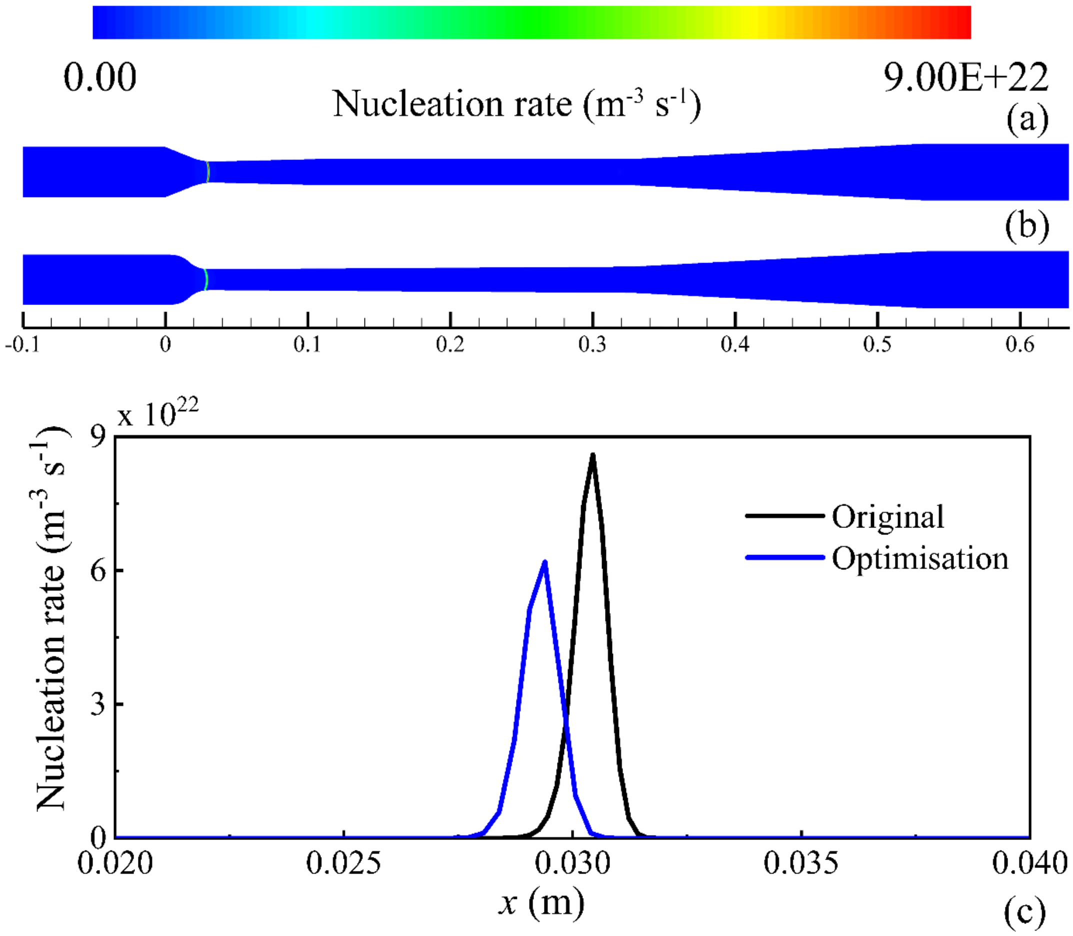

Fig. 15 Nucleation rate in original and optimised supersonic separators: contours of the original geometry (a), contours of the optimised geometry (b) and profiles of the original and optimised geometries (c)

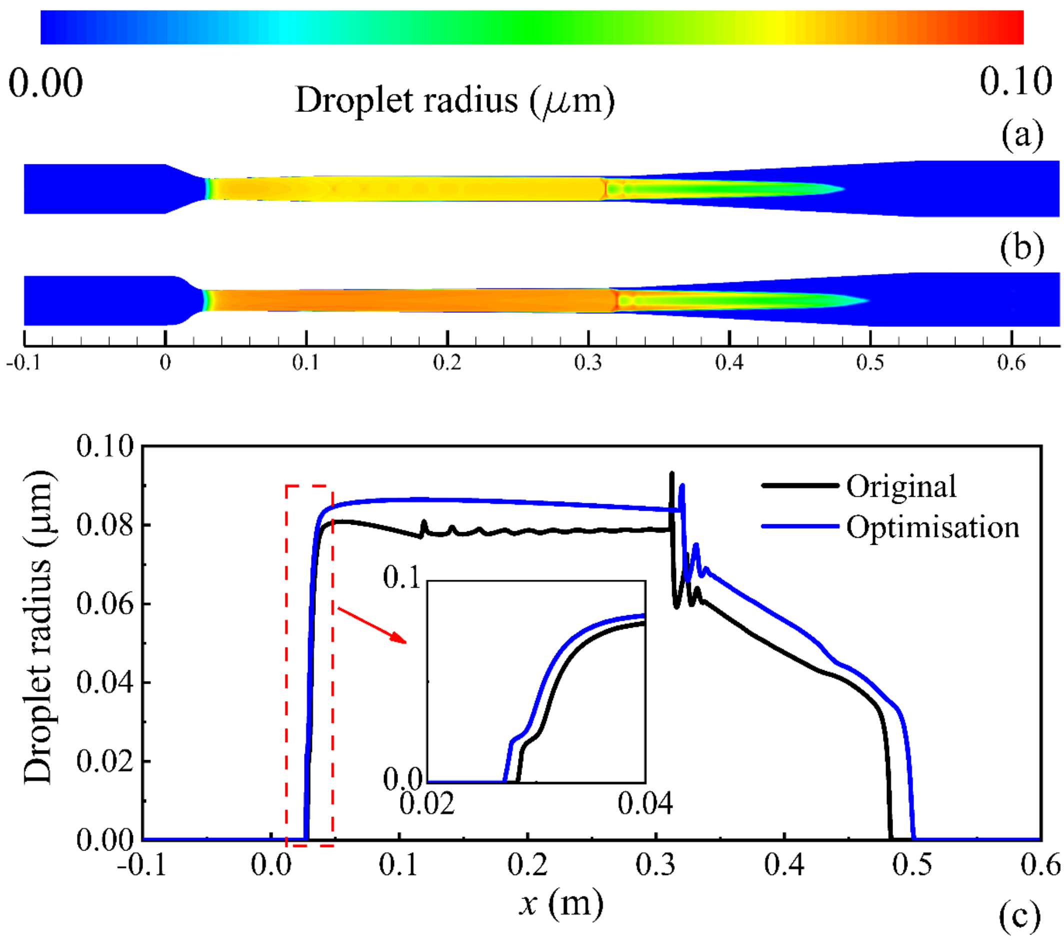

Fig. 16 Droplet radius in original and optimised supersonic separators: contours of the original geometry (a), contours of the optimised geometry (b) and profiles of the original and optimised geometries (c)

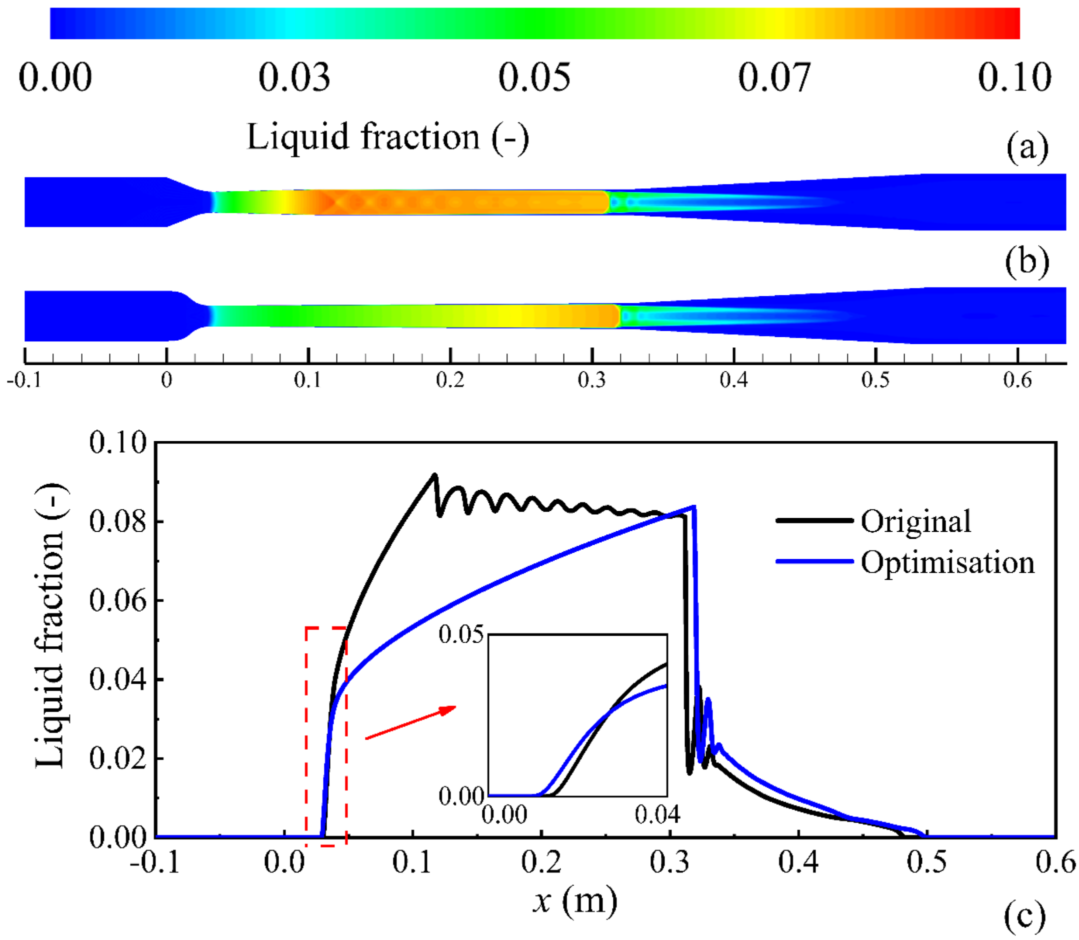

Fig. 17 Liquid fraction in original and optimised supersonic separators: contours of the original geometry (a), contours of the optimised geometry (b) and profiles of the original and optimised geometries (c)

3.5. Two-dimensional axisymmetric and three-dimensional simulations

As there is a query that the supersonic separator is simplified to the two-dimensional simulation in this study, the two-dimensional (2D) axisymmetric and three-dimensional (3D) simulations are carried out for the optimised supersonic separator. The 3D geometry of the supersonic separator is shown in Fig. 18. The flow features, such as the contours and profiles of the Mach number and the liquid fraction are described in Figs. 19-20 based on the 2D axisymmetric and 3D simulations. It can be seen that similar results are obtained from the 2D and 3D simulations, while there are some differences between them. The 3D simulation moves the position of the shock wave tiny upstream compared to the 2D simulation. The position of the shock wave locates at x = 0.317 m for the 3D case, while the shock wave occurs at x = 0.320 m for the 2D simulation. Subsequently, the different expansion levels of the vapour in the supersonic separator are observed that the vapour expands further for the 2D simulation with the maximum Mach number of approximately 1.60, while the 3D simulation predicts the maximum one of about 1.56.

The significant differences are observed downstream the shock waves for the 2D and 3D simulations of the optimised supersonic separators. It can be seen that both these two cases achieve almost the same Mach number near the exit plane of the separator although the Mach number predicted by 3D case declines more quickly than the 2D axisymmetric case. Furthermore, the liquid fraction decreases to zero at x = 0.406 m for the 3D simulation while it disappears at x = 0.498 m for the 2D simulation. This indicates that both 2D and 3D simulations predict the re-evaporation of the condensed droplets.

In general, both the 2D axisymmetry and 3D simulations predict very similar results upstream the shock wave with tiny different shock positions. The differences downstream shock waves do not affect the separation performance significantly for these 2D and 3D cases. Therefore, the 3D simulation for the supersonic separator can be reflected by the 2D axisymmetric modelling, which is acceptable considering the computational cost and time.

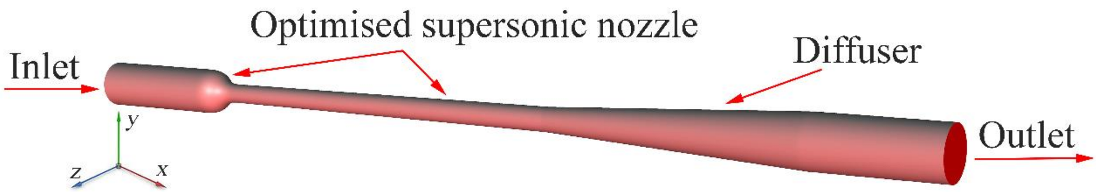

Fig. 18 Three-dimensional geometry of the optimised supersonic separator.

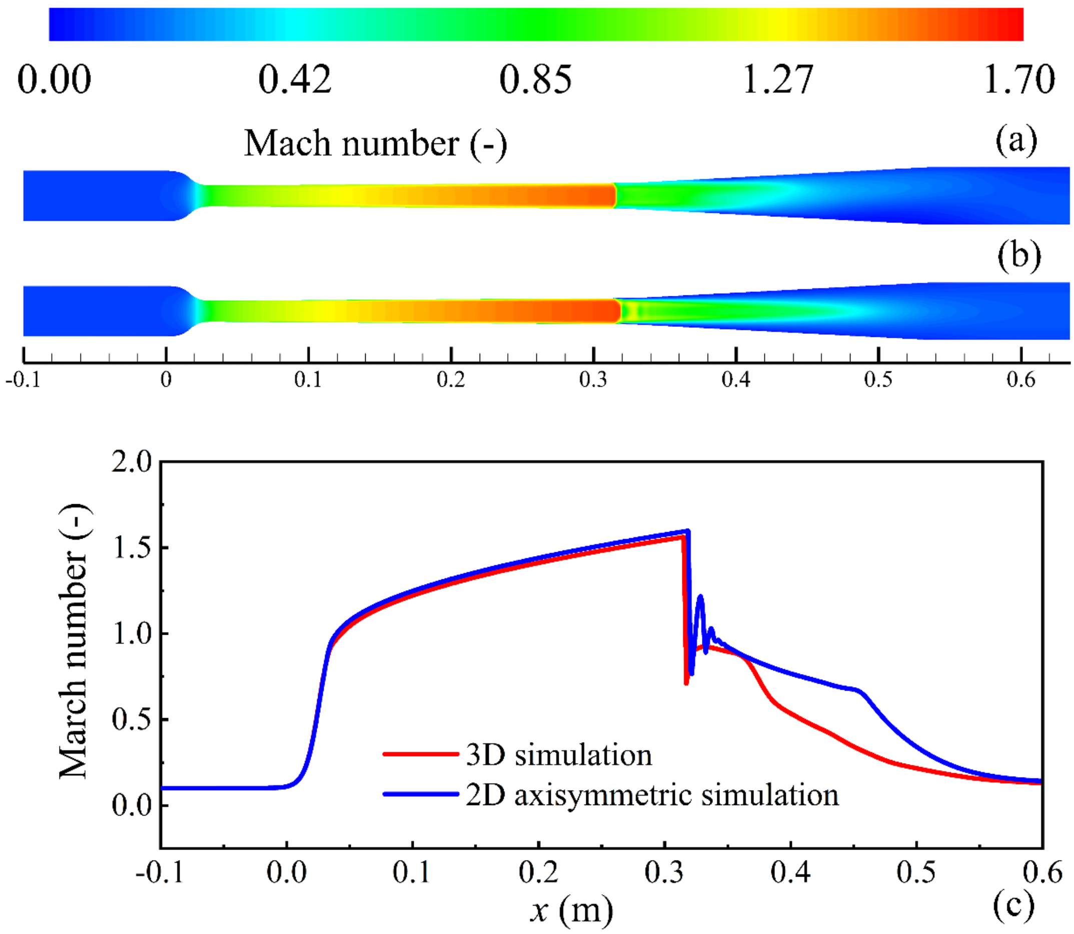

Fig. 19 Mach numbers in two-dimensional axisymmetric and three-dimensional supersonic separators: contours of the three-dimensional simulation (a), contours of the two-dimensional axisymmetric simulation (b) and profiles of the two-dimensional axisymmetric and three-dimensional simulations (c)

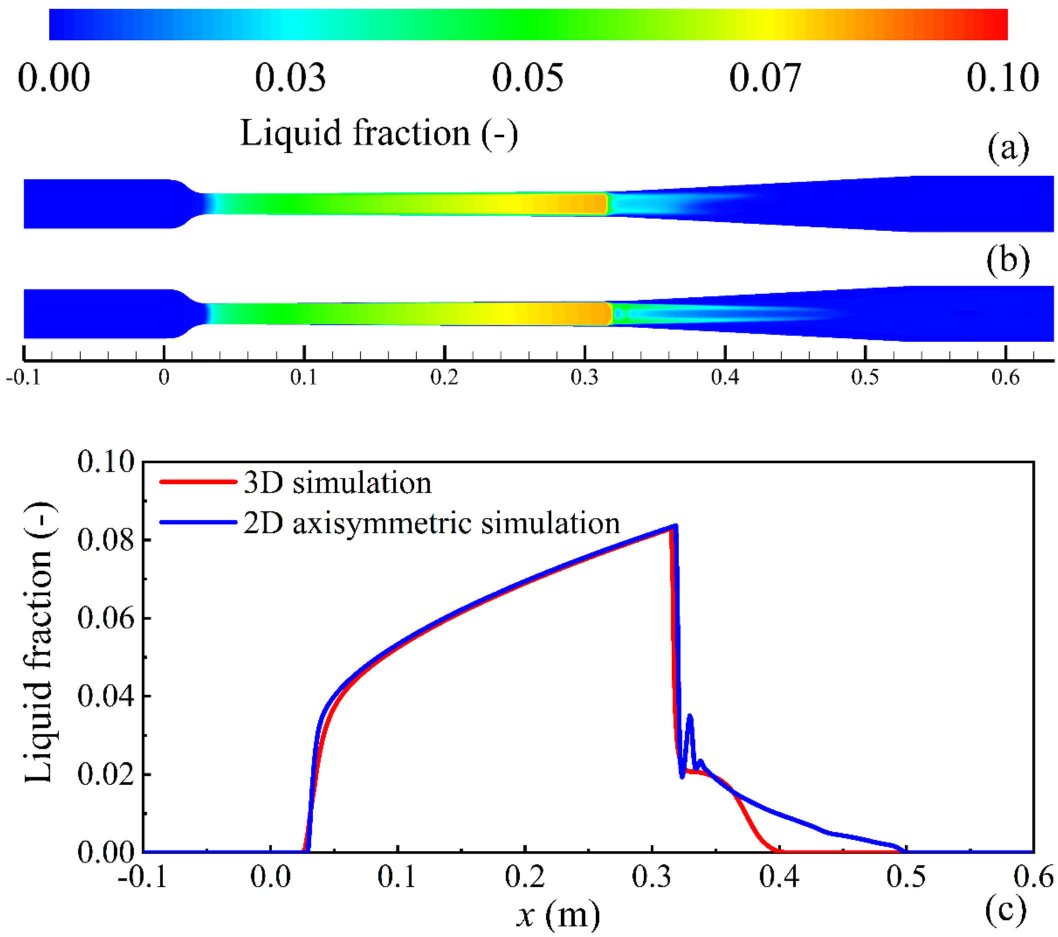

Fig. 20 Liquid fractions in two-dimensional axisymmetric and three-dimensional supersonic separators: contours of the three-dimensional simulation (a), contours of the two-dimensional axisymmetric simulation (b) and profiles of the two-dimensional axisymmetric and three-dimensional simulations (c)

4. Conclusions

The computational fluid dynamics modelling is developed for the performance evaluation of the supersonic separator. The single-phase flow model with an assumption of the dry gas stream causes unlimited decreases of the static pressure and temperature regardless of the saturation effect. The condensing flow model computes a liquid fraction of approximately 9.2% of the total mass, which influences the heat and mass transfer behaviour during the phase change process of water vapour in the supersonic separator.

The supersonic separator is optimised based on the idea of combining the nozzle diverging part and the constant tube as a long diverging part of the optimised nozzle. The optimised supersonic separator can improve the separation performance by a) eliminating oblique and expansion waves, b) inducing an earlier onset of the nucleation rate and generating larger droplets, and c) moving downstream the shock position and weakening the intensity of the shocks.

The present study ignores a swirling flow in a supersonic separator and a two-dimensional axisymmetric model is employed to focus on the phase change of water vapour. The impact of the swirling flow on the condensation process in a supersonic separator based on the three-dimensional model will be carried out in future studies.

Conflict of interest

The authors declared that there is no conflict of interest.

Acknowledgements

This project has received funding from the European Union's Horizon 2020 research and innovation programme under the Marie Sklodowska-Curie grant agreement No 792876 and the National Natural Science Foundation of China under Grant 51876143.

References

[1] E. Villicaña-García, J.M. Ponce-Ortega. Sustainable strategic planning for a national natural gas energy system accounting for unconventional sources. Energy Conversion and Management. 181 (2019) 382-97.

[2] P.H. Niknam, D. Fiaschi, H.R. Mortaheb, B. Mokhtarani. Numerical investigation of multiphase flow in supersonic separator considering inner body effect. Asia-Pacific Journal of Chemical Engineering. 14 (2019).

[3] X. Cao, J. Bian. Supersonic separation technology for natural gas processing: A review. Chemical Engineering and Processing-Process Intensification. 136 (2019) 138-51.

[4] R. Secchi, G. Innocenti, D. Fiaschi. Supersonic Swirling Separator for natural gas heavy fractions extraction: 1D model with real gas EOS for preliminary design. Journal of Natural Gas Science and Engineering. 34 (2016) 197-215.

[5] M. Castier. Effect of side streams on supersonic gas separations. Journal of Natural Gas Science and Engineering. 35 (2016) 299-308.

[6] C. Wen, N. Karvounis, J.H. Walther, H. Ding, Y. Yang. Non-equilibrium condensation of water vapour in supersonic flows with shock waves. International Journal of Heat and Mass Transfer. 149 (2020) 119109.

[7] E.I. Jassim. Geometrical Impaction of Supersonic Nozzle on the Dehumidification Performance During Gas Purification Process: an Experimental Study. Arabian Journal for Science and Engineering. 44 (2019) 1057-67.

[8] J. Bian, X. Cao, W. Yang, M.A. Edem, P. Yin, W. Jiang. Supersonic liquefaction properties of natural gas in the Laval nozzle. Energy. 159 (2018) 706-15.

[9] M. Castier. Modeling and simulation of supersonic gas separations. Journal of Natural Gas Science and Engineering. 18 (2014) 304-11.

[10] Y. Yang, C. Wen. CFD modeling of particle behavior in supersonic flows with

strong swirls for gas separation. Separation and Purification Technology. 174 (2017) 22-8.

[11] D. Majidi, F. Farhadi. Effect of the Wet Outlet Geometry on the Shockwave Position in Supersonic Separators. Chemical Engineering & Technology. 43 (2019) 126-36.

[12] D. Hu, Y. Wang, C. Ma. Numerical simulation of supersonic separator with axial or tangential outlet in reflow channel. Chemical Engineering and Processing - Process Intensification. 124 (2018) 109-21.

[13] S.H. Rajaee Shooshtari, A. Shahsavand. Numerical investigation of water droplets trajectories during natural gas dehydration inside supersonic separator. Journal of Natural Gas Science and Engineering. 54 (2018) 131-42.

[14] Q.-F. Ma, D.-P. Hu, J.-Z. Jiang, Z.-H. Qiu. A turbulent Eulerian multi-fluid model for homogeneous nucleation of water vapour in transonic flow. International Journal of Computational Fluid Dynamics. 23 (2009) 221-31.

[15] Q.-F. Ma, D.-P. Hu, J.-Z. Jiang, Z.-H. Qiu. Numerical study of the spontaneous nucleation of self-rotational moist gas in a converging–diverging nozzle. International Journal of Computational Fluid Dynamics. 24 (2010) 29-36.

[16] J. Bian, X. Cao, W. Yang, X. Song, C. Xiang, S. Gao. Condensation characteristics of natural gas in the supersonic liquefaction process. Energy. 168 (2019) 99-110.

[17] J. Bian, X. Cao, W. Yang, D. Guo, C. Xiang. Prediction of supersonic condensation process of methane gas considering real gas effects. Applied Thermal Engineering. 164 (2020) 114508.

[18] W. Sun, X. Cao, W. Yang, X. Jin. Numerical simulation of CO2 condensation process from CH4-CO2 binary gas mixture in supersonic nozzles. Separation and Purification Technology. 188 (2017) 238-49.

[19] W. Sun, X. Cao, W. Yang, X. Zhao. CFD modeling on non-equilibrium condensation process of H2S in CH4-H2S mixture expansion through supersonic nozzles. Fuel Processing Technology. 170 (2018) 53-63.

[20] S.H. Rajaee Shooshtari, A. Shahsavand. Reliable prediction of condensation rates for purification of natural gas via supersonic separators. Separation and Purification Technology. 116 (2013) 458-70.

[21] S.H.R. Shooshtari, A. Shahsavand. Maximization of energy recovery inside supersonic separator in the presence of condensation and normal shock wave. Energy. 120 (2017) 153-63.

[22] P.H. Niknam, H. Mortaheb, B. Mokhtarani. Dehydration of low-pressure gas using supersonic separation: Experimental investigation and CFD analysis. Journal of Natural Gas Science and Engineering. 52 (2018) 202-14.

[23] Y. Yang, C. Wen, S. Wang, Y. Feng, P. Witt. The swirling flow structure in supersonic separators for natural gas dehydration. RSC Advances. 4 (2014) 52967-72.

[24] C. Wen, N. Karvounis, J.H. Walther, Y. Yan, Y. Feng, Y. Yang. An efficient approach to separate CO2 using supersonic flows for carbon capture and storage. Applied energy. 238 (2019) 311-9.

[25] A. Li, A.C.Y. Yuen, T.B.Y. Chen, C. Wang, H. Liu, R. Cao, et al. Computational

Study of Wet Steam Flow to Optimize Steam Ejector Efficiency for Potential Fire Suppression Application. Applied Sciences. 9 (2019) 1486.

[26] C. Wen, H. Ding, Y. Yang. Performance of steam ejector with nonequilibrium condensation for multi-effect distillation with thermal vapour compression (MED-TVC) seawater desalination system. Desalination. 489 (2020) 114531.

[27] H. Ding, Y. Li, E. Lakzian, C. Wen, C. Wang. Entropy generation and exergy destruction in condensing steam flow through turbine blade with surface roughness. Energy Conversion and Management. 196 (2019) 1089-104.

[28] X. Han, W. Zeng, Z. Han. Investigating the dehumidification characteristics of the low-pressure stage with blade surface heating. Applied Thermal Engineering. 164 (2020) 114538.

[29] A. Kantrowitz. Nucleation in very rapid vapor expansions. The Journal of chemical physics. 19 (1951) 1097-100.

[30] J. Young. The spontaneous condensation of steam in supersonic nozzle. Physico Chemical Hydrodynamics. 3 (1982) 57-82.

[31] J. Starzmann, F.R. Hughes, S. Schuster, A.J. White, J. Halama, V. Hric, et al. Results of the International Wet Steam Modeling Project. Proceedings of the Institution of Mechanical Engineers, Part A: Journal of Power and Energy. 232 (2018) 550-70.

[32] ANSYS Fluent Theory Guide. ANSYS Inc, USA. (2017).

[33] Y. Yang, J.H. Walther, Y. Yan, C. Wen. CFD modeling of condensation process of water vapor in supersonic flows. Applied Thermal Engineering. 115 (2017) 1357-

62.

[34] F.R. Menter. Two-equation eddy-viscosity turbulence models for engineering applications. AIAA journal. 32 (1994) 1598-605.

[35] C. Wen, B. Rogie, M.R. Kærn, E. Rothuizen. A first study of the potential of integrating an ejector in hydrogen fuelling stations for fuelling high pressure hydrogen vehicles. Applied Energy. 260 (2020) 113958.

[36] S. Dykas, W. Wróblewski. Numerical modelling of steam condensing flow in low and high-pressure nozzles. International Journal of Heat and Mass Transfer. 55 (2012) 6191-9.

[37] Y. Yang, X. Zhu, Y. Yan, H. Ding, C. Wen. Performance of supersonic steam ejectors considering the nonequilibrium condensation phenomenon for efficient energy utilisation. Applied Energy. 242 (2019) 157-67.

[38] A. Jarrahian, E. Heidaryan. A new cubic equation of state for sweet and sour natural gases even when composition is unknown. Fuel. 134 (2014) 333-42.

[39] A. Jarrahian, E. Heidaryan. A simple correlation to estimate natural gas viscosity. Journal of Natural Gas Science and Engineering. 20 (2014) 50-7.

[40] A. Jarrahian, H.R. Karami, E. Heidaryan. On the isobaric specific heat capacity of natural gas. Fluid Phase Equilibria. 384 (2014) 16-24.

[41] A. Jarrahian, E. Heidaryan. A simple correlation to estimate natural gas thermal conductivity. Journal of Natural Gas Science and Engineering. 18 (2014) 446-50.

[42] C.A. Moses, G.D. Stein. On the growth of steam droplets formed in a Laval nozzle using both static pressure and light scattering measurements. Journal of Fluids

Engineering. 100 (1978) 311-22.

[43] H. Gürbüz, D. Buran. Experimental study on the effect of concentrated turbulence around the spark plug zone in a swirling flow on a hydrogen SI engine performance and combustion parameters. Journal of Energy Engineering. 142 (2016) 04015031.

[44] H. Gürbüz. Experimental evaluation of combustion parameters with ion-current sensor integrated to fast response thermocouple in SI engine. Journal of Energy Engineering. 143 (2017) 04016046.

[45] Ö. Solmaz, H. Gürbüz, M. Karacor. Comparison of Artificial Neural Network and Fuzzy Logic Approaches for the Prediction of In-Cylinder Pressure in a Spark Ignition Engine. Journal of Dynamic Systems, Measurement, and Control. 142 (2020) 091005.